Journal of Neuroscience Research 85:3673–3686 (2007)

Intrinsic Membrane Properties and Morphological Characteristics of Interneurons in the Rat Supratrigeminal Region

Chie-Fang Hsiao, Kelly Gougar, J. Asai, and Scott H. Chandler*

Department of Physiological Science and the Brain Research Institute, University of California at Los Angeles, Los Angeles, California

The membrane properties and morphological features of interneurons in the supratrigeminal area (SupV) were studied in rat brain slices using whole-cell patch clamp recording techniques. We classified three morphological types of neurons as fusiform, pyramidal, and multipolar and four physiological types of neurons according to their discharge pattern in response to a 1-sec depolarizing current pulse from −80 mV. Single-spike neurons responded with a single spike, phasic neurons showed an initial burst of spikes and were silent during the remainder of the stimulus, delayed-firing (DF) neurons exhibited a slow depolarization and delay to initial spike onset, and tonic (T) neurons showed maintained a discharge throughout the stimulus pulse. In a subpopulation of neurons (10%), membrane depolarization to around −44 mV produced a rhythmic burst discharge (RB) that was associated with voltage-dependent subthreshold membrane oscillations. Both these phenomena were blocked by the sodium channel blocker riluzole at a concentration that did not affect the fast transient spike. Low doses of 4-AP, which blocks low-threshold K^+ currents, transformed bursting into low-frequency tonic discharge. In contrast, bursting occurred with exposure to cadium, a calcium-channel blocker. This suggests that persistent sodium currents and low-threshold K^+ currents have a role in intrinsic burst generation. Importantly, RB cells were most often associated with multipolar neurons that exhibited either a DF or a T discharge. Thus, the SupV contains a variety of physiological cell types with unique morphologies and discharge characteristics. Intrinsic bursting neurons form a unique group in this region.

Key words: mastication; bursting; central pattern generator; jaw movement; oscillations

Oral-motor activities such as mastication, suckling, and swallowing are essential for mammals to survive. Yet knowledge of the neuronal basis for these behaviors lags behind that gained from studies of locomotion and respiration. A substantial amount of data has been accumulated on the circuitries, neurotransmitters, and receptor subtypes that initiate and carry out oral-motor reflexes (reviewed in Lund, 1991; Nakamura and Katakura, 1995), but the central circuits responsible for rhythmic oral-motor behaviors are not well understood. Specifically, rhythmic masticatory movements are believed to be under the control of brain stem circuits, referred to as central pattern generators (CPGs), that, when activated, produce masticatory or suckling type movements in the absence of phasic peripheral inputs (Goldberg and Chandler, 1990; Lund, 1991; Nakamura and Katakura, 1995). Based on transection experiments using either intact (Chandler and Tal, 1986) or highly reduced (Kogo et al., 1996; Tanaka et al., 1999) en bloc preparations, the minimal region of the brain stem that can produce rudimentary rhythmic output resides between the rostral poles of the trigeminal and facial motor nuclei. In intact preparations, many trigeminal nuclei in these regions in the vicinity of the trigeminal motor nucleus (TMN) exhibit a rhythmic discharge associated with a particular phase of the rhythmic jaw-movement cycle induced by central cortical or brain-stem stimulation (Donga and Lund, 1991; Inoue et al., 1992, 1994; Westberg et al., 1998).

The supratrigeminal region is a cluster of neurons that border the dorsal cap of the TMN (reviewed in Kamogawa et al., 1994) and, according to immunohistochemical and electrophysiological studies, contains excitatory and inhibitory interneurons, many of which project to the TMN (Goldberg and Nakamura, 1968; Turman and Chandler, 1994a,b; Li et al., 2005; among others). Historically, this region has received much attention for its role in producing glycinergic inhibition

Contract grant sponsor: National Institute of Dental and Craniofacial Research; Contract grant number: DE 06193.

*Correspondence to: Dr. Scott H. Chandler, PhD, Department of Physiological Science, UCLA, 2859 Slichter Hall, Los Angeles, CA 90095. E-mail: schandler@physci.ucla.edu

Received 2 April 2007; Revised 9 May 2007; Accepted 21 May 2007

Published online 1 August 2007 in Wiley InterScience (www.interscience.wiley.com). DOI: 10.1002/jnr.21442

of jaw-closer motoneurons during jaw-opening reflexes (Goldberg and Nakamura, 1968; Kidokoro et al., 1968). However, neurons in this region are rhythmically active during fictive mastication in intact rats (Inoue et al., 1992) and likely participate in some aspect of oral-motor pattern generation.

Moreover, others recently recorded a small population of neurons in the supratrigeminal region (SupV) from brain-stem slice preparations (Bourque and Kolta, 2001) and in other trigeminal interneuronal areas (Brocard et al., 2006; Min et al., 2003) that exhibit intrinsic rhythmic-bursting capabilities. These studies neither determined the ionic basis of SupV bursting nor conducted a detailed examination of the relationship between cell morphology and discharge pattern. In the present study we found a wide variety of discharge properties of neurons in the SupV region. However, a small percentage of neurons showed conditional, voltage-dependent intrinsic bursting that depended not on a negative slope conductance in the steady-state *I–V* relationship but on a persistent sodium current (I_{NaP}) and a 4-AP-sensitive K^+ current. Although we found that SupV neurons varied in morphology and discharge patterns, rhythmically bursting neurons were found only in multipolar neurons that exhibited either a tonic or a delayed-firing pattern. Some aspects of this data were presented previously (Hsiao et al., 2003).

MATERIALS AND METHODS

Preparation for Whole-Cell Recording

Whole-cell patch clamp experiments were performed on neurons from coronal slices of 8- to 12-day-old neonatal rat brain stem. This age was chosen because conversion from suckling to rudimentary adultlike mastication begins during this period (Westneat and Hall, 1992). Furthermore, this is when neuronal changes occur in preparation for this conversion, such as ligand-gated or intrinsic burst generation in both Mes V neurons and trigeminal motoneurons (Wu et al., 2001; Hsiao et al., 2002), development of inward rectification (Tanaka et al., 2003), and modification of NMDA subunit expression (Turman et al., 1999). Animal protocols were approved by the Institutional Animal Care and Use Committee at UCLA. Rats were anesthetized by 2-bromo-2-chloro-1,1,1-trifluoroethane inhalation (Sigma, St. Louis, MO). The brain was removed and placed in oxygenated ice-cold cutting solution. Coronal sections (300 μm) through the trigeminal motor nucleus (TMN) were obtained and then placed in the incubation solution at 37°C for 30 min.

Solutions

Solutions were bubbled with 95% O_2/5% CO_2 and maintained at a pH of 7.25–7.3 (22°C–24°C). The cutting solution was composed of 126 mM NaCl, 3 mM KCl, 1.25 mM NaH_2PO_4, 26 mM $NaHCO_3$, 10 mM glucose, 1 mM $CaCl_2$, 5 mM $MgCl_2$, and 4 mM lactic acid. The recording solution consisted of 124 mM NaCl, 3 mM KCl, 1.25 mM NaH_2PO_4, 26 mM $NaHCO_3$, 10 mM glucose, 2 mM $CaCl_2$, and 2 mM $MgCl_2$. The incubation solution was identical to the recording solution except for the addition of 4 mM lactic acid. The composition of the solution used for isolating persistent sodium currents contained 131 mM NaCl, 10 mM HEPES, 3 mM KCl, 10 mM glucose, 1 mM $CaCl_2$, 2 mM $MgCl_2$, 10 mM tetraethylammonium chloride, 10 mM CsCl, 1 mM 4-AP, and 0.1 mM $CdCl_2$. The following drugs were added to the bath at the indicated concentrations: 5 μM riluzole, 200 μM $CdCl_2$, 50 μM 4-AP, 10 μM bicuculline methiodide, 10 μM strychnine, 10 μM APV, and 10 μM CNQX. All drugs were purchased from Sigma (St. Louis, MO). The normal pipette solution contained 115 mM K-gluconate, 9 mM NaCl, 25 mM KCl, 1 mM $MgCl_2$, 10 mM Hepes buffer, 0.2 mM EGTA, 3 mM K_2-ATP, and 1 mM Na-GTP, with a pH of 7.25–7.30 and osmolarity of 280–290 mOsm. The pipette solution used for recording the persistent sodium current was composed of 130 mM CsF, 9 mM NaCl, 10 mM HEPES, 10 mM EGTA, 1 mM $MgCl_2$, 3 mM K_2-ATP, and 1 mM Na-GTP, with a pH of 7.25–7.30 and osmolarity adjusted to 280–290 mOsm.

Whole-Cell Recording

Slices were perfused with oxygenated recording solution (2 mL/min) while secured in a recording well mounted on a Zeiss fixed-stage Axioskop microscope equipped with bright-field and fluorescence optics. Neurons were visualized with enhanced resolution using infrared differential video microscopy. Patch recordings were obtained with an Axopatch 1D (Axon Instruments, Foster City, CA) in concert with pCLAMP acquisition software (version 9.2, Medical Devices, Sunnyvale, CA) operating on a Pentium-based personal computer. Signals were digitized online, filtered at 2 kHz (voltage clamp) or 5–10 kHz (current clamp), and sampled at 10–50 kHz depending on the experiment. Patch pipettes were fabricated from conventional thin-walled glass (1.5 mm OD, 0.86 mm ID; Warner Instrument, Hamden, CT) and pulled on a Brown-Flaming P-97 micropipette puller (Sutter Instruments, Novato, CA). Their bath resistance was 3–5 MΩ. Signals were grounded by a 3M KCl agar bridge electrode (Ag/AgCl wire) mounted in the recording well. Liquid junction potentials were measured between the pipette and bath solutions and varied between 5 mV (normal pipette solution) and 7 mV (modified pipette solutions) and were corrected offline. Whole-cell capacitance (C_{inp}) was determined from the integral of capacity current in response to 15-msec hyperpolarizing voltage commands or directly obtained by the pCLAMP software during the experiment. Uncompensated series resistance (Rs) was calculated from the decay time constant (tau) of the transient and was usually less than 10 MΩ. Sixty-eighty percent compensation was routinely employed. Data were not collected in the first 10 min of gaining whole-cell access. Input resistance (R_{inp}) was determined from the slope of the steady-state *I–V* relationship in response to a series of voltage command steps from the resting potential. Various parameters of spike discharge frequency in response to a 1-sec current pulse were measured: instantaneous frequency for the first interspike interval and mean frequency, measured as the mean of the instantaneous frequency of each interval in a spike train. Adaptation

in a spike train was defined by an adaptation index (AI), calculated as: frequency of first spike interval − frequency of last interval)/mean frequency for all spikes in the response. A value greater than 1 indicated significant adaptation. The threshold for action potential initiation in response to a brief, 3-msec current pulse was defined as the membrane potential on the rising phase of the spike where the dV/dT inflection was most prominent. Subthreshold membrane potential oscillations just prior to the onset of rhythmic bursting or during the interburst periods of a bout of rhythmic bursting were quantified by fast Fourier transform (FFT) of the voltage region between two subsequent burst discharges. The FFT was constructed from 2-sec epochs. The results of three epochs were averaged.

Identification of Supratrigeminal Interneurons

The trigeminal motor nuclei in a coronal slice were identified bilaterally under low magnification (50×) as an opaque, pale oval region medial to the trigeminal principal sensory nucleus and ventral-lateral to the periaqueductal gray and central canal (Chandler et al., 1994). Following the identification of the TMN, the visual field was moved to an area within 400 μm dorsal to the border of the TMN. Supratrigeminal interneurons were visualized at higher magnification (400×) and clearly identified as neurons with small somata (around 15–30 μm) of various morphologies.

Following whole-cell patch clamp recording, one of three methods was used to label trigeminal interneurons for subsequent morphological analysis. In each method, after neurons were filled, slices were fixed for 24 hr at 4°C with 4% paraformaldehyde in 0.01M Tris-buffered saline (TBS, pH = 7.4). One set of neurons (n = 21 neurons) was injected with a 0.2% biocytin in the pipette solution and subsequently processed with a peroxidase-conjugated Avidin Biotin Complex kit (Vectastain Elite Standard Kit, Vector Laboratories, 1% Triton-X, TBS). Peroxidase activity was visualized with a solution of 2.3 mM 3,3′-diaminobenzidine tetrahydrochloride and 2.9 mM H_2O_2 in TBS. Morphological analysis of these neurons was conducted using a Zeiss Axioskop light microscope and its associated NIH Image software. Another set of interneurons (n = 6) was injected with a pipette solution containing 0.2% biocytin and subsequently processed using a fluorescein-streptavidin kit (Vector Laboratories; 30 μg/mL in 0.1M phosphate-buffered saline). The third set of interneurons (n = 20) was injected with Alexa Fluor 488 (Molecular Probes, Eugene OR). Following all histochemistry procedures, slices were mounted on slides, dried overnight, dehydrated, and coverslipped. Interneurons labeled with fluorescein or Alexa Fluor were analyzed using a Zeiss LSM 510 confocal microscope equipped with an argon laser (excitation at 488 nm). Three-dimensional reconstructions were created, thereby allowing spatial rotation and optimal morphological classification.

Retrograde Labeling of Trigeminal Motoneurons

In one set of experiments, rats received injections of Texas Red (10%, Molecular Probes, Eugene, OR) into the masseter muscle 4 days prior to electrophysiology experiments (n = 10 animals). Following the completion of electrophysiology and histochemical processing with either fluorescein-streptavidin or Alexa Fluor 488 (mg/mL), slices were viewed using a Zeiss LSM 510 confocal microscope utilizing argon lasers allowing excitation at 488 and 585 nm to view labeled interneurons (green) and retrogradely labeled trigeminal motoneurons (red), respectively. This double-labeling procedure allowed us to visualize the spatial relationship between labeled interneurons and the masseter motoneuronal pool.

The results are reported as means ± SEs. Comparisons of group means were performed with one-way analysis of variance (ANOVA) and Student t tests, with differences considered significant at $P < 0.05$ unless otherwise stated.

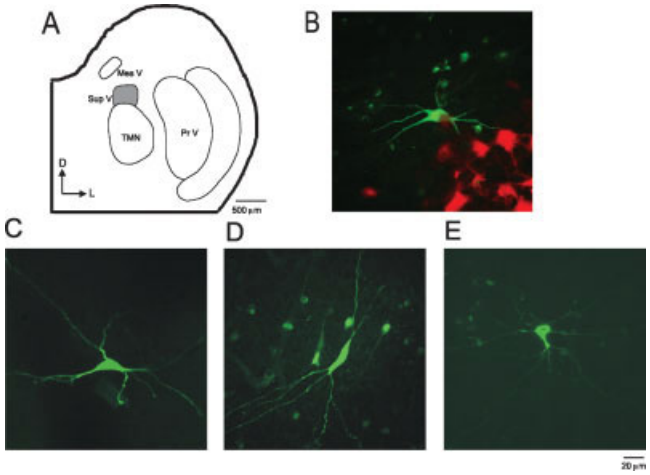

Fig. 1. Morphological characterization of SupV interneurons. **A:** Schematic drawing of region around trigeminal motor nucleus where SupV neurons were recorded (shaded area). **B:** Relationship between jaw-closer motoneuron pool and an SupV neuron labeled with Alexa Fluor. **C:** Pyramidal neuron. **D:** Fusiform neuron. **E:** Multipolar neuron. Each shows a three-dimensional confocal microscopic reconstruction of a recorded neuron labeled with Alexa Flour (488). Scale bar is the same for B–E (Mes V, mesencephalic V nucleus; TMN, trigeminal motor nucleus; PrV, principal sensory nucleus). [Color figure can be viewed in the online issue, which is available at www.interscience.wiley.com.]

RESULTS

The data presented in this article are based on patch clamp recordings from the supratrigeminal interneurons of P8–P12 rats. The initial criteria for inclusion into the database was resting potential greater than −50 mV, action potential amplitude exceeding 80 mV and input resistance of at least 100 MΩ. A total of 209 SupV interneurons were recorded. Figure 1A shows the region in the vicinity of the trigeminal motor nucleus to which we confined our recordings. For some analyses the data set was further reduced to 47 neurons that were successfully labeled and identified morphologically. A typical example of a labeled neuron in relationship to the dorsal lateral region of the TMN, as represented by

TABLE I. Membrane Properties of SupV Neurons According to Discharge Pattern and Morphological Classification

	Resting V_m (mV)	R_{inp} (MΩ)	C (pF)	AP amp (mV)	AHP amp (mV)	Threshold (mV)	Sag-amp (mV)
Physiological Cell types							
Delayed-firing (n = 73)	−57 ± 0.7	408 ± 20.6	59 ± 2.2	99 ± 1.2	6.6 ± 0.46	−42 ± 0.7^{**T}	4.3 ± 0.4
Phasic (n = 37)	−58 ± 1.0	378 ± 30.0	58 ± 2.4	99 ± 1.4	5.1 ± 0.56	−44 ± 1.0	3.4 ± 0.5
Single-Spike (n = 16)	−57 ± 1.8	396 ± 47.6	57 ± 4.5	94 ± 2.4	4.1 ± 0.81^{*D,T}	−45 ± 1.5	3.8 ± 0.7
Tonic (n = 83)	−58 ± 0.8	416 ± 21.7	60 ± 2.0	102 ± 1.3^{**S}	6.5 ± 0.51	−45 ± 0.6	4.4 ± 0.5
P	0.78	0.78	0.90	0.05	0.05	0.01	0.45
Morphological cell types							
Fusiform (n = 12)	−59 ± 1.6	403 ± 50.2	54 ± 5.6	97 ± 3.8	5.1 ± 1.12	−41 ± 2.8	4.2 ± 1.1
Pyramidal (n = 12)	−55 ± 1.7	397 ± 72.7	57 ± 3.2	97 ± 4.3	5.3 ± 0.91	−41 ± 1.9	3.5 ± 0.5
Multipolar (n = 23)	−57 ± 1.3	377 ± 42.1	63 ± 4.0	96 ± 2.8	5.9 ± 0.78	−44 ± 1.7	3.5 ± 0.4
P	0.25	0.93	0.32	0.93	0.79	0.40	0.63

P indicates 1-way ANOVA value. Data show means ± S.E.M. $^{*}p < 0.05$, $^{**}p < 0.01$ according to Fisher post hoc test. Abbreviations next to * indicate the group the comparison was made with. Vm is resting potential, Rinp is input resistance, C is total capacitance, AP amp is action potential amplitude, AHP amp is afterhyperpolarization peak amplitude, D is delayed-firing, T is tonic, S is single-spike. Threshold represents the voltage at which a 3 ms current pulse evokes an action potential. Sag-amp represents the voltage difference between the steady-state voltage at the end of a hyperpolarizing current pulse to −90 mV and the peak early voltage.

TABLE II. Summary of Morphological Parameters

	Fusiform	Pyramidal	Multipolar	P
Soma area (μm^2)	304.8 ± 33.7	264.7 ± 15.4	256.6 ± 20.2	0.27
Major axis (μm)	30.4 ± 2.6^{*M}	26.1 ± 1.4	23.1 ± 0.9	0.04
Minor axis (μm)	15.2 ± 1.3	16.5 ± 0.7	16.5 ± 0.7	0.55
Number of primary dendrites	2.7 ± 0.1^{**M}	3.5 ± 0.2	4.3 ± 0.2^{**P}	<0.01
Total cells	11	10	23	

P indicates 1-way ANOVA p value. Data show means ± S.E.M. $^{*}p < 0.05$, $^{**}p < 0.01$ according to Fisher post hoc test. Abbreviations next to P value indicate the group to which the comparison was made. M, multipolar. P, pyramidal.

the retrograde-labeled masseter motoneurons, is shown in Figure 1B.

Morphological Classification

The data from intracellular labeling indicate that supratrigeminal neurons can be classified morphologically into three types. Fusiform neurons showed elongated somas with processes stemming from each pole (Fig. 1C). Pyramidal cells had pyramid-shaped somas with three distinct poles, from which typically emanated a single process or occasionally two processes (Fig. 1D). Multipolar cells were defined as neurons with somas that had no consistent shape and three or more primary processes (Fig. 1E). If there were any discrepancies, emphasis was given to soma shape. Table I shows the morphological characteristics and electrophysiological properties of 47 neurons that were successfully labeled, whereas Table II summarizes the morphological characteristics of those labeled neurons. Table I also shows selected passive and active membrane properties for the total population of neurons ($n = 209$) according to neuron firing characteristics (described below).

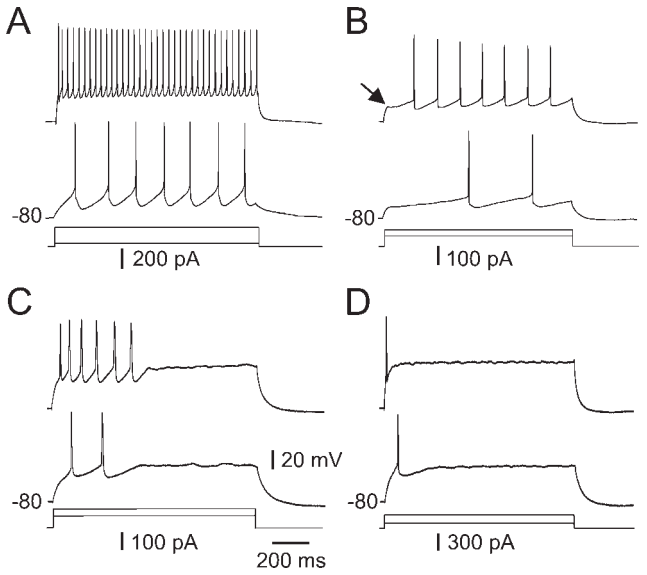

Fig. 2. Four types of discharge patterns identified for SupV interneurons. **A:** Tonic neuron. **B:** Delayed-firing neuron. **C:** Phasic neuron. **D:** Single-spike neuron. All neurons were held at −80 mV to remove inactivation.

Physiological Classification

We classified supratrigeminal neurons into four categories—tonic (T), delayed-firing (DF), phasic (P), and single-spike (SS)—according to their discharge pattern in response to a 1-sec depolarizing current pulse of different intensities from a holding membrane potential of −80 mV. Examples of the discharge pattern for each type of neuron are shown in Figure 2A–D.

Tonic neurons displayed a maintained frequency of discharge at rheobase, whereas delayed-firing neurons showed a slow ramp-like depolarization prior to the

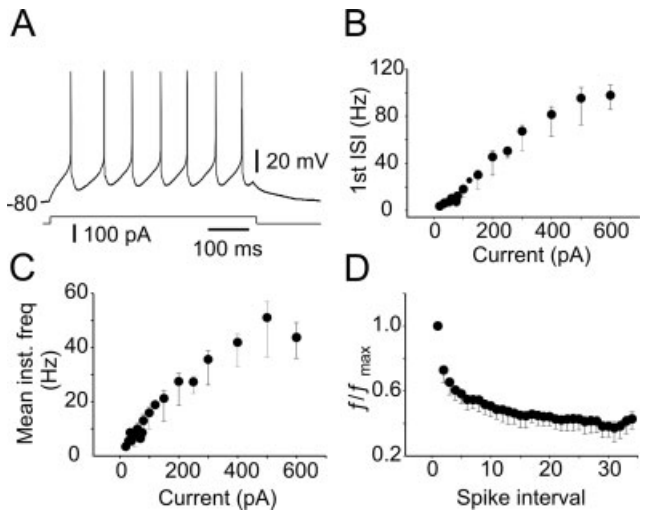

Fig. 3. Discharge characteristics of tonic neurons. **A:** Sample response. **B:** Summary composite plot ($n = 9$ neurons) for first ISI. **C:** Mean instantaneous frequency. **D:** Normalized instantaneous *freq*/$freq_{max}$ versus spike interval number (spike number in the train expressed as an ordinate). SE bars are indicated in each plot.

initial spike in response to a depolarizing current pulse applied from −80 mV. In most DF neurons, a small transient hyperpolarization (trough) at the onset of the pulse was observed [Figs. 2B and 5D (arrow)] with the larger stimulus intensities. At the rheobase, the delay to first spike was 593 ± 54 msec ($n = 9$), whereas at 40 pA above the rheobase, the delay was reduced to 153 ± 26 msec. Both types of neurons exhibited a relatively linear increase in frequency throughout the stimulus range examined until a maximum was reached. Figure 3 shows a composite summary of the frequency–current relationships for the first ISI (Fig. 3B) and mean instantaneous frequency (Fig. 3C) for the nine tonic neurons examined. Although not shown, the frequency–current relationships for DF neurons were qualitatively similar to those shown for tonic neurons. Both tonic and DF neurons showed some degree of spike adaptation during the spike train (Table III), as indicated by the normalized instantaneous frequency–spike interval relationship. The composite summary for the tonic neurons is shown in Figure 3D. In most cases, the normalized frequency–spike interval relationship for both groups of neurons was best fit with a single exponential function to determine the time constant (TC) of adaptation (tonic neurons: TC = 5.3 ± 0.90 msec, $n = 9$; DF neurons: TC = 7.1 ± 1.3 msec, $n = 8$). Table III lists the values of the pertinent discharge frequency parameters measured for each category of neuron.

Phasic neurons displayed an initial burst of action potentials in response to current injections and were silent during the remainder of the current pulse (Fig. 2C). Spike adaptation (Table III) was observed prior to spike cessation in most of these neurons. The mean TC of the 9 neurons measured was 1.3 ± 0.88 msec, which was significantly faster than that of the DF and tonic neurons (ANOVA, $P < 0.01$). Phasic neurons were also most prone to depolarization spike block. Typically, the maximal number of spikes was achieved within the first 100 pA of stimulation, and increasing the amplitude of the current pulse produced responses of diminishing amplitude with fewer spikes (not shown). Examination of all neurons according to firing mode showed that the minimal currents necessary to initiate a depolarization spike block (reduction in number and amplitude of the spikes in the spike train in response to increasing stimulus intensity) were: phasic, 207 ± 51.3 pA, $n = 9$; tonic, 406 ± 33.8 pA, $n = 9$; and DF, 422 ± 76.0 pA, $n = 9$; $P < 0.03$ as determined by ANOVA.

Single-spike neurons exhibited a solitary action potential at the onset of a depolarizing current pulse. Increasing the current intensity did not produce additional spikes (Fig. 2D). However, these neurons were also susceptible to a depolarization spike block at intensities above rheobase (not shown).

Table I summarizes some basic passive and active membrane properties of the different neuron types classified according to firing pattern. As indicated, there were significant differences in action potential amplitude, peak AHP amplitude, and voltage at spike threshold. Resting potential and cell size, inferred from R_{inp} and C_{inp}, respectively, did not differ significantly between groups and therefore could not account for these differences.

Table IV shows the distribution of neurons according to spike discharge pattern and cell morphology. As indicated, firing property classification was not correlated with morphology ($\chi^2 = 4.7$, $df = 6$, $P > 0.5$). However, Table IV does show some interesting trends. None of the 12 fusiform neurons exhibited single-spike discharge characteristics, and 16 of the 23 multipolar neurons (70%) exhibited either tonic discharge (8 neurons) or delayed firing (8 neurons) in response to a depolarizing current pulse.

Afterpotentials

Supratrigeminal neurons exhibited both monophasic (113 of 209 neurons, 54%; Fig. 4A) and multiphasic (96 of 209 neurons, 46%; Fig. 4B) afterhyperpolarization in response to a brief (3 msec) stimulus pulse from the resting potential. Monophasic afterhyperpolarization (AHP) was seen as a slowing of approximately the last one third of the action potential repolarization trajectory. This resulted in a slowly occurring long-duration AHP (sAHP) with a peak below the initial resting potential (6.2 ± 0.44 mV, $n = 113$). Those neurons that exhibited multiphasic afterpotentials were characterized by prominent afterdepolarization (ADP; 2.7 ± 0.33 mV, $n = 65$), which occurred on the down swing of the action potential that slowly declined into a sAHP (6.0 ± 0.35, $n = 96$). However, in a subset of multiphasic neurons ($n = 31$), a clear and prominent intervening ADP was absent or too small to unambiguously measure. Instead, a small depolarizing inflection on the spike

TABLE III. Frequency Parameters Analyzed by Discharge Pattern

	Max 1st ISI (Hz)	Mean max freq (Hz)	# APs	1st slope (Hz/pA)	Adaptation	Rheobase (pA)
Delayed-firing (n = 12)	89.2 ± 11.4	49.2 ± 5.3	35.0 ± 3.5	0.17 ± 0.19	1.05 ± 0.12	26.9 ± 4.8
Phasic (n = 12)	75.0 ± 10.4	66.0 ± 8.0	6.9 ± 1.2^{**D,T}	0.28 ± 0.05	0.92 ± 0.13	62.2 ± 14.9
Tonic (n = 12)	96.1 ± 9.5	51.5 ± 4.7	33.8 ± 4.4	0.23 ± 0.02	1.38 ± 0.10^{*P,D}	44.5 ± 9.7
P	0.36	0.13	<0.0001	0.11	0.03	0.08

P indicates 1-way ANOVA p value. Data show means ± S.E.M. *p < 0.05, **p < 0.01 according to Fisher post hoc test. Abbreviations next to * indicate the group to which the comparison was made. D, delayed-firing. P, phasic. T, tonic.

TABLE IV. Distribution of Numbers of Neurons According to Discharge Pattern and Morphological Classification

	Fusiform	Pyramidal	Multipolar
Tonic	5	3	8
Delay-firing	3	3	8
Phasic	4	3	4
Single-spike	0	3	3

Chi square P > 0.05, DF = 6.

repolarization that immediately developed into a sAHP was observed. When the neurons were segregated according to discharge pattern, only 32% of phasic neurons and 25% of single-spike neurons exhibited multiphasic afterpotentials compared with 55% of tonic neurons and 47% of delayed-firing neurons ($\chi^2 = 8.56$, $df = 3$, $P \leq 0.04$; Fig. 4C). With respect to morphology, 11 of the 12 fusiform neurons exhibited monophasic AHPs, unlike the other morphological types, for which a correlation with firing pattern was not found.

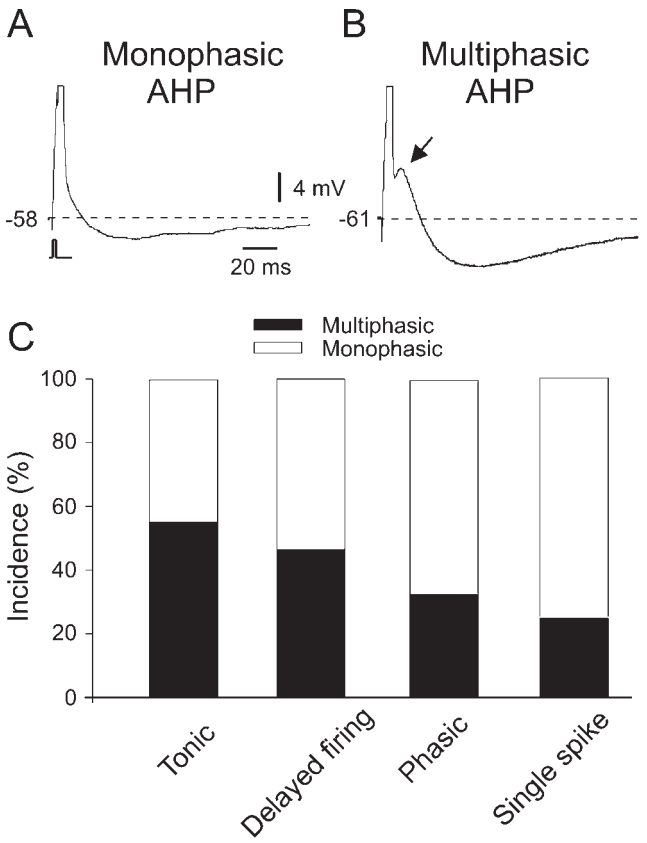

Fig. 4. Afterhyperpolarization (AHP) in SupV interneurons. **A:** Monophasic AHP. **B:** Multiphasic AHP with prominent afterdepolarization (ADP, arrow). **C:** Bar chart of incidence (percentage) of monophasic (white bars) and multiphasic (black bars) AHP according to cell discharge pattern. $P < 0.05$ for chi-square test of spike pattern versus AHP type, $df = 3$. Note truncated action potentials in A and B.

Ionic Mechanisms Underlying Single-Spike and Phasic Neuron Discharge Patterns

Our previous studies of mesencephalic V neurons (Mes V) showed that a steady-state, low-threshold 4-AP sensitive K^+ current is responsible for the rapid adaptation and spike cessation observed in those neurons in response to a suprathreshold current pulse (Del Negro and Chandler, 1997; Wu et al., 2001). To determine if similar mechanisms underlie the strong adaptation in both single-spike and phasic neurons, we applied low doses of 4-AP (<50 μM) and then examined the discharge characteristics in response to depolarizing current pulses. Figure 5 shows typical examples of the effects of 4-AP on the discharge pattern of a single-spike and a phasic neuron. For both types of neurons, the discharge pattern was transformed into a tonic pattern after 50 μM 4-AP ($n = 4$).

Phasic neurons typically showed a few spikes prior to cessation of discharge during the pulse and exhibited some degree of spike adaptation during discharge (Fig. 5B). After 4-AP application, rheobase was lower, and spike discharge was maintained at a frequency *lower* than that of the control for the duration of the current pulse (Fig. 5B). This was true for both the first ISI (control max frequency = 25.0 ± 3.0 Hz vs. 4-AP max frequency = 15.6 ± 2.3 Hz, $n = 4$, $P < 0.05$) and the mean instantaneous frequency of discharge during the pulse (control = 19.2 ± 2.4 Hz vs. 4-AP = 11.7±1.4 Hz, $n = 4$, $P < 0.05$; Fig. 5C). In addition, the degree of adaptation was significantly reduced (4 of 4 neurons; Fig. 5C, right). For all of the single-spike and phasic neurons, spike duration was prolonged after 4-AP (Fig. 5B), suggesting participation of a 4-AP-sensitive K^+ current in spike repolarization. These data suggest a low-threshold, noninactivating 4-AP-sensitive K^+ current underlies the strong adaptation and early spike termination observed in both single-spike and phasic neurons. This was further supported by the prominent outward rectification at depolarized potentials observed in the

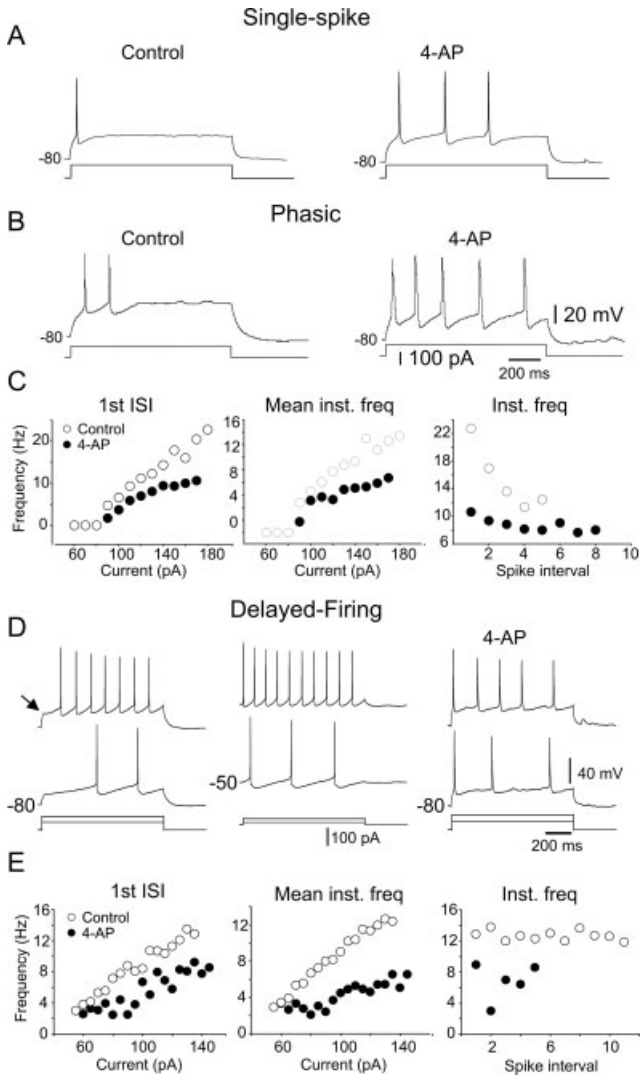

Fig. 5. 4-AP-sensitive currents sculpt the discharge patterns of single-spike, phasic, and delayed-firing neurons. **A:** Single-spike neurons generated only one spike in response to a current pulse from −80 mV and multiple spikes in the presence of 4-AP. **B:** Discharges of a phasic neuron before and during 4-AP application. **C:** Left, frequency–current plots of first ISI; middle, frequency–current plot of mean instantaneous frequency before (open circles) and after (filled circles) application of 4-AP; right, instantaneous frequency versus spike interval. **D:** Delayed-firing neurons, characterized by a slow ramp depolarization prior to spike onset from a holding potential of −80 mV (arrow). **D:** Middle, discharge pattern of same neuron after adjustment of membrane potential to −50 mV; right, discharge pattern of same neuron after adjustment of the membrane potential to −80 mV and during application of 4-AP (50 μM). Note no delay to onset of spike discharge after 4-AP. **E:** Left, frequency–current plot of first ISI; middle, frequency–current plot of mean instantaneous frequency before (open circles) and during (filled circles) 4-AP exposure conditions for a delayed-firing neuron. **E:** Right, instantaneous frequency versus spike interval number for the same neuron.

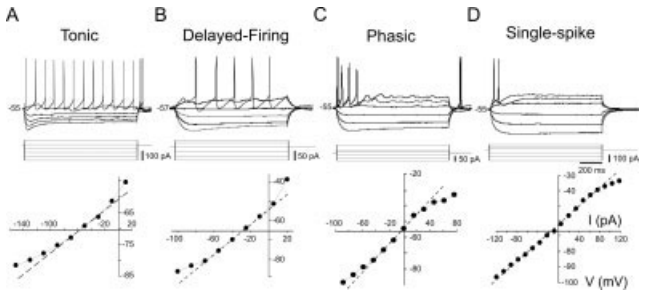

Fig. 6. Subthreshold voltage-current relationships for SupV interneurons according to discharge pattern. Above, representative raw data evoked by 1-sec current pulses for each neuron type; below, steady-state V-I relationships at end of the step pulse. The dotted line is the linear regression fit to the data taken around the resting potential. Membrane rectification is indicated by a deviation from the fit line. **A:** Tonic neuron (PIR occurred after termination of the pulse). **B:** Delayed-firing neuron. **C:** Phasic neuron (PIR occurred after termination of the pulse). **D:** Single-spike neuron.

steady-state *V–I* relationship in the absence of 4-AP (Fig. 6C,D).

Mechanism Underlying Delayed-Firing Pattern

As previously shown, delayed-firing neurons were characterized by a considerably delayed onset to the first spike in response to a depolarizing current pulse from a hyperpolarized holding potential (Fig. 5D, left). At holding potentials more depolarized from approximately −50 mV, the initiation of the first spike was almost immediate, and sustained discharge ensued, as shown in Figure 5D (middle). This suggests that an underlying voltage-dependent, transient outward K^+ current, an A-type current (reviewed in Coetzee et al., 1999), mediates the delayed-discharge pattern. In all four SupV neurons examined, application of 50 μM 4-AP produced similar results (Fig. 5D, right). Figure 5E shows an example of the effects of 4-AP on the frequency–*I* relationship for a DF neuron. In contrast with that observed for single-spike and phasic neurons, the change in frequency after 4-AP was quite variable. In two neurons the frequency of the first ISI and mean steady-state frequency decreased throughout the current range tested (Fig. 5E), whereas for the other two neurons the frequency either remained the same or increased.

Membrane Rectification and Postinhibitory Rebound

Passive and active membrane properties were further studied in a subpopulation of neurons. Voltage-current plots indicate further differences between neuron types based on firing pattern (Fig. 6). For instance, all single-spike and phasic neurons showed strong depolarizing steady-state *outward* rectification at voltages slightly more depolarized from resting potential. This was indicated by the deviation from linearity (dashed line) in the

V–I plot (Fig. 6C,D, bottom). In contrast, just prior to the rheobase, the tonic and DF neurons showed a small degree of *inward* rectification in the steady-state *V–I* relationship (Fig. 6A,B) never seen in single-spike or phasic neurons.

Hyperpolarizing inward rectification was observed in most neurons regardless of morphological classification or firing type. This was seen as a sag in the membrane voltage toward resting potential at the most hyperpolarized potentials and a deviation from linearity in the *V–I* plot (Fig. 6). This response is typically associated with an underlying h current (I_h), as shown in the Mes V neurons (Khakh and Henderson, 1998; Tanaka et al., 2003). Table I indicates the values for the sag amplitude (steady-state amplitude − early peak amplitude measured at −90 mV) according to cell classification. For the entire population the amplitude was small (4.2 ± 0.25 mV, $n = 209$) compared with that of Mes V neurons, which typically show a prominent sag greater than 10 mV at similar voltages (Tanaka et al., 2003). When the database was reduced to those neurons showing a sag amplitude of 2 mV or greater, ($n = 145$), significant differences were found between cell types according to firing pattern, but not morphology ($P < 0.05$ by ANOVA). The largest sag amplitude was found for tonic cells (6.4 ± 0.54, $n = 51$), followed by DF neurons (5.2 ± 0.40, $n = 54$), single-spike neurons (4.7 ± 0.7, $n = 12$), and phasic neurons (4.4 ± 0.57, $n = 25$).

Postinhibitory rebound (PIR) is an important membrane response to promote rhythmic burst discharge in many types of neurons in the CNS (Reyes, 2001; Migliore and Shepherd, 2002; Paz, 2005). Trigeminal Mes V neurons show a prominent PIR mediated by the inward rectifier, I_h (Khakh and Henderson, 1998; Tanaka et al., 2003; Wu et al., 2005), as well as by a persistent sodium current (Wu et al., 2005). Because most supratrigeminal neurons exhibited some degree of sag at the largest hyperpolarizing potentials, we explored the possibility that those neurons would exhibit PIR as well. For the total population of neurons examined, regardless of firing pattern or morphology, 106 of 209 neurons (51%) exhibited PIR spikes at the termination of a large hyperpolarizing pulse to approximately −90 mV (Fig. 6A,C). This value marginally increased to 54% for the population of neurons that showed a sag amplitude of at least 2 mV. However, there was no significant correlation of the presence of PIR with firing pattern or with morphology. Nevertheless, the mean amplitude of the sag potential was approximately 38% greater in the PIR neuron population than in the non-PIR population, suggesting some contribution to PIR from an I_h current (PIR group, 4.7 ± 0.38, $n = 106$, vs. non-PIR group, 3.4 ± 0.28, $n = 101$; $P < 0.01$ by Student unpaired *t* test).

Burst Discharge in SupV Interneurons

The ability of supratrigeminal neurons to produce maintained conditional bursting, that is, bursting in response to maintained membrane depolarization in the absence of pharmacological activation, was examined in 209 neurons. For the total population, approximately 10% (21 of 209 neurons) showed conditional burst generation, and these neurons were distributed uniformly in the SupV.

The bursting neurons showed a clear rhythmic burst pattern in response to maintained membrane depolarization, which we termed rhythmic bursting (RB). These neurons showed a maintained tonic spike discharge during the intraburst period, with clearly defined interburst silences during a bursting sequence (Fig. 7A). For the remaining 188 neurons, prolonged membrane depolarization did not produce any form of maintained burst discharge but instead produced either single-spike (Fig. 7B) or irregularly occurring tonic discharge during the maintained stimulus. Comparisons of some passive membrane properties in the bursting and nonbursting neurons indicated that RB neurons had a significantly more negative resting potential (−61.5 ± 1.5 mV, $n = 21$, vs. −57.0 ± 0.45 mV, $n = 188$; $P \leq 0.01$), lower input resistance (323 ± 33.4 MΩ, $n = 21$, vs. 413 ± 13.7 MΩ, $n = 188$; $P \leq 0.05$) and greater membrane capacitance (68.0 ± 3.6 pF, $n = 21$, vs. −57.6 ± 1.3 pF, $n = 188$; $P \leq 0.01$) compared with nonbursting neurons. Rhythmic bursting still occurred in the presence of antagonists for glycine, GABA, and excitatory amino acids, suggesting that they were indeed intrinsic in nature (Fig. 7D).

The mean threshold for burst initiation occurred at −44.3 ± 0.7 mV ($n = 21$), and the mean cycle period and burst duration for the group were 3.3 ± 0.44 and 1.14 ± 0.20 sec, respectively. The mean coefficient of variation for the burst cycle period for all RB neurons examined was 0.32% ± 0.029%, suggesting that the burst periodicity was fairly regular. The mean intraburst spike frequency for the population of recorded neurons measured at the most stable membrane potential for bursting for each neuron (between −43 and −38 mV) was 7.5 ± 0.59 Hz ($n = 21$). In some experiments the voltage dependence of intraburst spike frequency, burst-cycle duration, and burst duration were examined. As shown in Figure 7C, spike frequency in a burst showed voltage dependence ($P < 0.01$ as determined by ANOVA, $n = 7$); however, in the narrow voltage range for which these neurons rhythmically burst, there was no significant relationship between membrane voltage and cycle burst period or duration. In most cases, strong depolarization transformed the bursts into tonic discharge or produced spike inactivation and cessation of activity.

Similar to that observed for Mes V neurons (Wu et al., 2001), during rhythmic bursting, spiking did not occur on a wave of membrane depolarization or plateau potential. This is in contrast to that observed during NMDA/5-HT-induced bursting in trigeminal motoneurons or that recently shown in trigeminal sensory nucleus neurons (Brocard et al., 2006), suggesting a lack of a prominent negative slope conductance in the steady-state *I–V* relationship for SupV neurons. Furthermore,

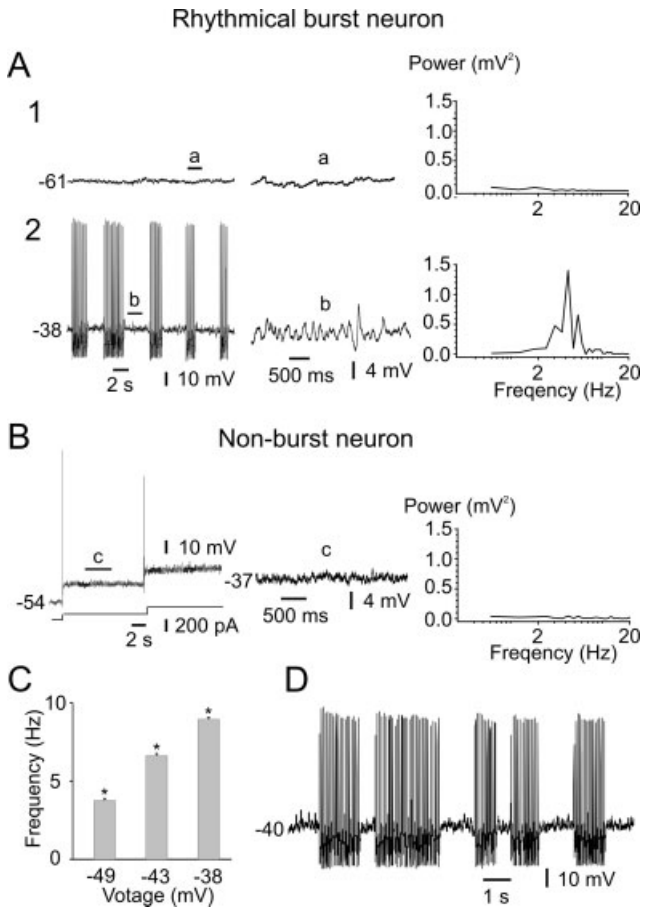

Fig. 7. Discharge characteristics and subthreshold membrane properties of bursting and nonbursting neurons. **A:** Subthreshold and discharge characteristics of a rhythmic burst neuron. (1) Left record, voltage trace at resting potential (−61 mV); middle record, labeled a, region of membrane potential at faster time base and higher magnification; right, fast Fourier transform (FFT) of the membrane potential from left record. (2) Rhythmic burst discharge from the same neuron held at −38 mV. Middle record, region of membrane potential during interburst interval marked b; right, plot of power spectrum of the membrane potential with a dominant frequency at 8 Hz. **B:** Same as A, except for a nonbursting neuron held at −54 mV. Note the lack of maintained spike discharge and low-amplitude subthreshold oscillations. FFT plot shown on right is on the same scale as that shown in A. **C:** Composite histogram of 7 neurons of intraburst spike frequency at different membrane potentials (*significantly different from −49 mV for intraburst frequency, as determined by ANOVA; $P < 0.001$ for each comparison according to Fisher post hoc test). **D:** Rhythmic burst discharge in the presence of strychnine (10 μM), bicucculline (10 μM), CNQX (10 μM), and APV (10 μM).

during the interburst period, the membrane potential did not show a large postburst hyperpolarization. In fact, the membrane potential at termination was similar to that seen just prior to burst onset [Fig. 7A(2)]. Similar to that observed in Mes V neurons during bursting, a voltage-dependent increase in subthreshold membrane potential fluctuation was observed during the interburst period (Fig. 7A, middle traces) that was not prominent in nonbursting neurons at a similar membrane potential (Fig. 7B, middle). Typical power spectra (FFT) of subthreshold membrane potential activity during the interburst periods for an RB neuron at resting potential (−61 mV) and at a more depolarized level (−38 mV) are shown in Figure 7A(1,2). At membrane potentials subthreshold for bursting, the amplitude of the membrane potential fluctuations was small but increased with membrane depolarization [Fig. 7A(2), middle]. In bursting neurons around resting potential, the power spectra for membrane potential fluctuation showed a small peak with low power at a frequency around 2 Hz (2.5 ± 0.4 Hz, $n = 8$; Fig. 7A(1), right). In some cases, a wide peak around 0.2–0.4 Hz was also evident. However, when those neurons were depolarized from resting potential to approximately −40 mV, the predominate peak was shifted to higher frequencies and exhibited greater power (6.2 ± 0.87 Hz, $n = 8$, $P \leq 0.004$; Fig. 7A(2), right). In nonbursting neurons at approximately −40 mV, the amplitude of the subthreshold oscillations was smaller, and the power spectra typically showed a smaller peak at frequencies around 4 Hz (3.8 ± 0.36 Hz, $n = 9$; compare Fig. 7A,B, middle), which is lower than that found in burst neurons ($P \leq 0.02$ by unpaired Student t test). In the presence of antagonists for glutamate, glycine, and GABA, the subthreshold oscillations were still present (Fig. 7D) and voltage-dependent in 8 of 10 neurons examined, suggesting they were indeed intrinsic and not a result of synaptic potentials.

TABLE V. Distribution of Burst Cells According to Discharge Pattern and Morphology

	Fusiform	Pyramidal	Multipolar	Tonic	Delay	Phasic	Single-spike
RB	0	0	3	13	7	1	0
NB	12	12	20	70	66	36	16

P value for Chi square test for morphology ($p = 0.19$, DF = 2) or discharge pattern vs burst mode ($p = 0.07$, DF = 3).

Relationship between Bursting, Firing Pattern, and Morphology

We next sought to determine if there was a relationship between the tendency of neurons to burst and either morphology or firing pattern. Table V indicates some significant trends. RB neurons (3 of 47 labeled neurons) were found only in multipolar neurons, suggesting they are associated with a distinct neuron morphology. We next examined the relationship between bursting and firing pattern regardless of morphology. Interestingly, we found that single-spike and phasic neurons seldom exhibited any form of bursting (1 of 21 neurons), whereas most RB neurons (20 of 21, 95%) were associated with tonic or DF neurons (Table V). These data suggest that rhythmic-bursting neurons are mainly associated with multipolar neurons that discharge in tonic or DF mode.

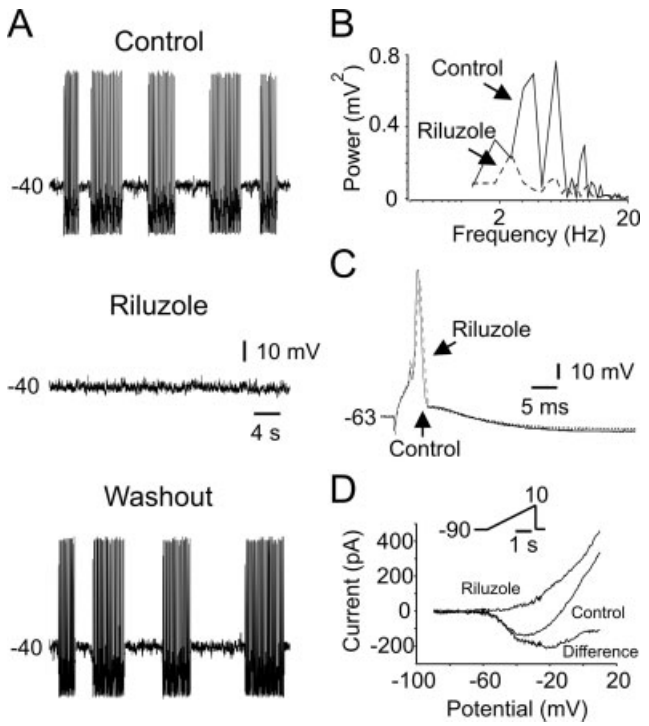

Fig. 8. Persistent Na^+ currents participate in generation of bursting activity in SupV interneurons. **A:** Rhythmic burst discharge evoked by constant depolarizing current injection and abolished by application of riluzole (5 μM). **B:** Plot showing FFT analysis of membrane potential during interburst periods prior to and during riluzole application. **C:** Single-spike evoked by a short pulse (3 msec) before (dashed line) and after riluzole. **D:** Effect of riluzole on I_{NaP} evoked by a slow (14 mV/sec) depolarizing voltage ramp from −90 to +10 mV in control solution and in the presence of riluzole. Note the complete block of inward current after riluzole. Data were leak subtracted. Inset shows command voltage protocol.

Mechanism for Burst Generation

To investigate the potential role of various levels of ionic conductance in the generation of interneuron bursting activity, we examined the effects of various antagonists previously used to study the mechanisms of burst generation in other types of trigeminal neurons (Wu et al., 2001, 2005). Previously, we showed that persistent sodium currents (I_{NaP}), in conjunction with slowly or noninactivating potassium currents are responsible for burst activity in Mes V neurons (Wu et al., 2001, 2005). Therefore, to determine if similar mechanisms applied to supratrigeminal neurons, we examined the effects of riluzole, an antagonist of I_{NaP} (Urbani and Belluzzi, 2000; Wu et al., 2005) on interneuron rhythmic burst activity. Figure 8A shows an example of such an experiment. In the presence of riluzole, rhythmic bursting was not possible regardless of membrane potential level. In all five neurons examined, riluzole (5 μM) completely abolished stimulus-induced rhythmic burst activity and suppressed subthreshold oscillations, as indicated by the FFT having a significant shift in peak frequency (control, 5.5 ± 0.73 Hz, vs. riluzole, 2.6 ± 0.37 Hz; $P < 0.01$, $n = 5$) and reduction in power (control, 0.66 ± 0.14, vs. riluzole, 0.3 ± 0.07; $P < 0.05$). A typical example is shown in Figure 8B (dashed line). However, under these conditions, a brief stimulus pulse could still induce an action potential (Fig. 8C), thus excluding the possibility that suppression of rhythmic bursting resulted from direct suppression of fast activations of sodium channels. Suppression of bursting was reversible after a 15- to 20-min washout (Fig. 8A, bottom).

To determine directly if riluzole suppressed I_{NaP} in supratrigeminal neurons, voltage clamp experiments were performed. Figure 8D shows the typical effect of riluzole on I_{NaP} evoked by a slow (14 mV/sec) ramp voltage command, from −90 to +10 mV. In the five neurons examined, the peak instantaneous inward current was completely blocked and showed only outward rectification. These data indicate that, similar to bursting in Mes V neurons, persistent Na^+ currents are important for generation of subthreshold oscillations and bursting activity in SupV interneurons.

In Mes V neurons, low doses of 4-AP (50 μM) block low-threshold, slowly, and noninactivating K^+ currents, and these currents are critical for burst generation in those neurons (Wu et al., 2001, 2005). Therefore, we examined the effects of low doses of 4-AP on burst generation in supratrigeminal neurons. Figure 9A shows a typical bursting pattern in control conditions and in the presence of 4-AP. In all five neurons examined, burst activity was transformed into a low-frequency tonic discharge with minimal effects on the fast action potential after drug application. Furthermore, examination of 4-AP in all five neurons showed that it only reduced the AHP peak amplitude during a burst by an average of 7.7% ± 0.03% ($P < 0.06$ by paired Student t test; Fig. 9B, top) and that it significantly reduced the AHP, by an average of 19.3% ± 0.05%, following an action potential evoked by a 3-msec current pulse from resting potential ($P < 0.04$; Fig. 9B, bottom).

In contrast to 4-AP, block of calcium currents with $CdCl_2$ (200 μM), a nonselective Ca^{2+} channel antagonist, did not block bursting (Fig. 9C) but did reduce the peak AHP in a burst (mean reduction of 69.2% ± 0.03%, $P \leq 0.001$ by paired Student t test, $n = 5$ neurons; Fig. 9D, top) and the peak AHP (89.0% ± 0.04% reduction; $P \leq 0.001$ by paired Student t test) induced by a single short current pulse (3 msec, 5 of 5 neurons; Fig. 9D, bottom). As shown, these effects were reversible. In 3 of 5 neurons Cd^{2+} decreased burst cycle duration, whereas in 4 of 5 neurons burst duration decreased and spike frequency increased after drug application. These results suggest that Ca^{2+} currents are not important for the generation of rhythmic bursting activity but do participate in controlling spike frequency and sculpting the discharge pattern, most likely via modulation of calcium-dependent AHP.

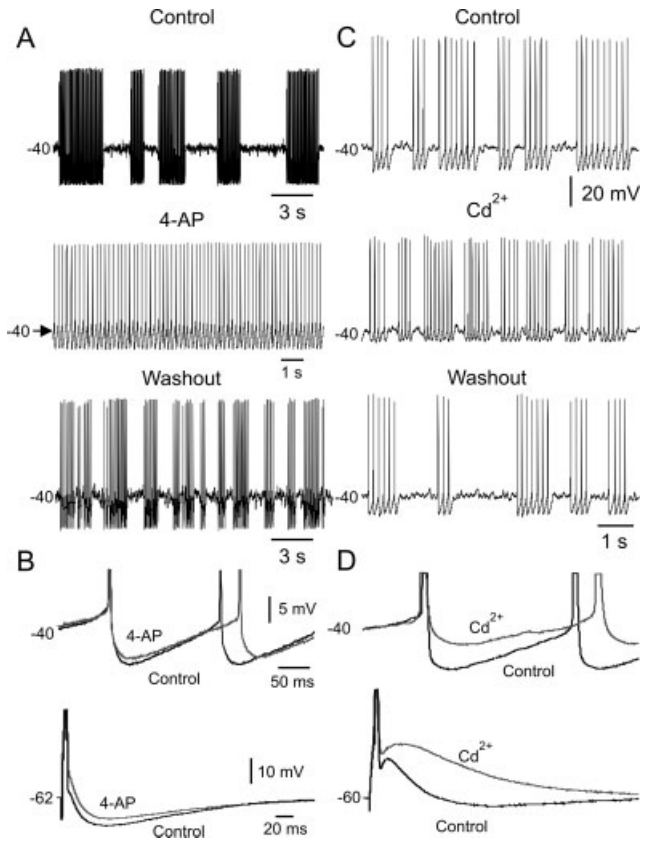

Fig. 9. Effects of ion channel blockers on bursting and spike discharge characteristics. **A:** Application of 4-AP (50 μM) transformed the rhythmic burst discharge into low-frequency tonic spiking. **B:** Top, superimposition of first two spikes in a burst before (black) and after (gray) application of 4-AP (note minimal effects on AHP amplitude); bottom, single-spike evoked by a short step pulse (3 msec) before (black dotted line) and after (gray dotted line) application of 4-AP. **C:** Effects of Cd^{2+} on bursting and spike discharge characteristics. **D:** Top, same as **B** except in the presence of 200 μM Cd^{2+} (note reduction in AHP); bottom, same as **B,** except in the presence of Cd^{2+} (note reduction in AHP amplitude, thus exposing an ADP).

DISCUSSION

Characterization of both intrinsic membrane properties and discharge characteristics for the varied groups of trigeminal interneurons is critical for understanding how trigeminal neuronal circuits receive, integrate, and produce context-dependent oral-motor patterns. Although we have a reasonably good understanding of the neuronal circuits responsible for a number of oral-motor reflexes (see Lund, 1991; Nakamura and Katakura, 1995), the precise identity of the constituent neurons of the central circuits, known as central pattern generators (CPGs), underlying oral-motor rhythmic movements such as suckling and mastication remain elusive. Nevertheless, progress has been made in defining (1) the minimal regions of the brain stem compatible with oral-motor rhythmic activity (Chandler and Tal, 1986; Tanaka et al., 1999), (2) synaptic interconnections between trigeminal interneuronal nuclei in those regions (Mizuno, 1970; Rokx et al., 1986; Bourque and Kolta, 2001), and (3) intrinsic membrane properties and discharge characteristics of neurons in those regions (Inoue et al., 1992, 1994; Bourque and Kolta, 2001; Min et al., 2003; among others). In the present study we found that a small population of SupV neurons exhibit conditional burst-generating properties that are most associated with multipolar neurons that discharge in either tonic or delayed-firing mode. The basis for this bursting is dependent on a nontraditional bursting mechanism that does not depend on negative slope conductance in the steady-state *I–V* relationship, but rather on activation of both I_{NaP} and 4-AP-sensitive low-threshold K^+ currents.

Neurons in the supratrigeminal region are important constituents controlling aspects of oral-motor activity because they (1) project to the trigeminal motor nucleus (Mizuno et al., 1983), (2) respond to oral-sensory stimulation (Goldberg and Namamura, 1968; Kidokoro et al., 1968), and (3) are rhythmically active during fictive mastication (Miyazaki and Luschei, 1987; Inoue et al., 1992). Clearly, they are in a unique position to integrate oral-motor sensory information with signals from oral-motor central pattern generators (CPGs). Furthermore, although the precise nature of the circuits that make up the oral-motor CPG are not known, these neurons are within the narrow boundaries of the minimal brain-stem regions compatible with rhythmic oral-motor activity (Chandler and Tal, 1986; Tanaka et al., 1999) and have extensive connections with other trigeminal nuclei (Bourque and Kolta, 2001; Li et al., 2005), suggesting they could be constituents of the CPG.

Firing Properties of SupV Neurons

The four types of discharge patterns observed are similar to those described for interneurons in other trigeminal (Bourque and Kolta, 2001; Min et al., 2003) and spinal cord (Prescott and De Koninck, 2002; Szucs et al., 2003; Smith and Perrier, 2006; among others) nuclei. Although passive membrane properties were not significantly correlated with discharge properties (Bourque and Kolta, 2001; Min et al., 2003), some differences between neurons according to discharge mode were apparent. Tonic and DF neurons are clearly distinct from each other and from SS and P neurons, but it was difficult to determine if SS and P neurons form unique neuronal types or are part of a continuum. Furthermore, SS and P neurons showed strong steady-state outward rectification, which most likely accounts for the strong adaptation observed. In addition, they were more likely to have smaller amplitude monophasic, as opposed to multiphasic, AHPs compared to those in T and DF neurons. Tonic and DF neurons, in contrast, typically showed steady-state inward rectification prior to spike threshold. Furthermore, DF neurons were easily distinguished by their characteristic voltage-dependent prolonged

latency to the initial spike onset around the rheobase, which was blocked in the presence of 4-AP. This would indicate the presence of an A-type potassium current in those neurons, similar to that shown in trigeminal motoneurons (Hsiao and Chandler, 1995). In addition, the characteristic discharge patterns of SS and P neurons were transformed into those resembling tonic neurons after 4-AP application, suggesting an underlying slowly inactivating or noninactivating low-threshold potassium current (Del Negro and Chandler, 1997). The varied discharge patterns observed were not surprising, given that this nucleus integrates complex sensorimotor signals arising from both central and peripheral sources (Mizuno et al., 1983; Yasui et al., 1985; Inoue et al., 1992; Minkels et al., 1995).

Bursting Neurons and Subthreshold Oscillations

Neurons that discharge in a burst-generating mode are important for information transfer between neurons (Lisman, 1997; Izhikevich et al., 2003). We found that approximately 10% of SupV neurons exhibited conditional bursting when the membrane potential was depolarized continuously from the resting potential. These neurons exhibited regular and maintained rhythmic burst discharge, with a relatively low coefficient of variation ($\sim$ .3) during bursting. The results for this group of neurons are not too dissimilar from those previously recorded in peritrigeminal neurons with sharp electrodes (Bourque and Kolta, 2001), or parvocellular reticular neurons using the patch method (Min et al., 2003).

RB neurons were characteristically associated with voltage dependent subthreshold membrane oscillations that increased in amplitude and frequency at depolarized membrane potential levels and were suppressed by riluzole, which blocks persistent sodium currents in other trigeminal neurons (Wu et al., 2005). In some respects, these oscillations resembled those observed in Mes V neurons during conditional burst discharge (Wu et al., 2001, 2005) or in other types of neurons in the central nervous system (Boehmer et al., 2000; Hamam et al., 2002; Bracci et al., 2003; Reboreda et al., 2003). It is likely that the onset of bursting is triggered by the membrane instability generated by the subthreshold oscillations, as was shown for Mes V neurons (Wu et al., 2001) and striatal neurons (Bracci et al., 2003). Subthreshold oscillations of similar frequency and pharmacological sensitivity to SupV neurons were reported in cultured dorsal column nuclei (Reboreda et al., 2003) and striatal fast-spiking neurons (Bracci et al., 2003), among others, and were proposed to facilitate synchronization of populations of related neurons during burst discharge.

Mechanisms of Burst Generation

We found that bursting is dependent on riluzole-sensitive persistent sodium currents and a 4-AP sensitive K^+ current, similar to that previously characterized for Mes V neurons (Wu et al., 2001). In contrast, bursting was maintained, although in a modified form, in the presence of Ca^{2+} antagonists. In addition, SupV neurons do not produce plateau potentials during burst activity or exhibit a negative slope conductance in their steady-state I–V relationship, similar to that found in other CNS neurons (Roper et al., 2004). This makes them different than ''traditional'' burst-generating cells such as trigeminal motoneurons during NMDA- or 5-HT-induced bursting (Hsiao et al., 1998; Del Negro et al., 1999) or than trigeminal principal V sensory neurons during maintained membrane depolarization that exhibit plateau potentials (Sandler et al., 1998; Brocard et al., 2006).

SupV Neuron Bursting Requires Persistent Sodium Currents

Parvocellular and peritrigeminal neurons caudal to TMN show calcium-dependent bursting (Min et al., 2003). In the present study, removal of calcium (not shown) or application of cadmium to block calcium currents altered the burst pattern but did not eliminate rhythmic bursting. Furthermore, it is unlikely that PIR and the underlying h current associated with rhythmic bursting in other CNS neurons (McCormick and Pape, 1990) participate in SupV intrinsic bursting, since maintained bursting occurred at very depolarized potentials ($\sim$40–45 mV), and the afterhyperpolarization following each spike within or between bursts did not bring the membrane potential into the region of I_h activation, which typically is close to -70 mV in other trigeminal neurons (Tanaka et al., 2003).

In contrast, reduction of persistent sodium currents with riluzole readily abolished bursting, similar to that found in Mes V neurons (Wu et al., 2005) and in burst-generating neurons in the trigeminal principal sensory nucleus (Brocard et al., 2006). Furthermore, riluzole suppressed the voltage-dependent subthreshold oscillations, similar to that observed in Mes V and other CNS neurons (Reboreda et al., 2003; Wu et al., 2005). It is clear that I_{NaP} currents are important constituents of bursting neurons of other rhythmogenic networks (reviewed in Ramirez et al., 2004; Feldman and Del Negro, 2006). Modulation of these channels by various neuromessengers provides a means to fine-tune and sculpt the output of pattern-generating networks.

Relationship between Bursting, Morphology, and Discharge Patterns

Supratrigeminal neurons exhibited three distinct types of morphologies: fusiform, pyramidal, and multipolar. A previous study (Bourque and Kolta, 2001) reported only fusiform and triangular neurons in peritrigeminal regions, whereas we also found multipolar neurons, which made up slightly less than half the labeled neurons. This difference in findings could have been a result of the differences between the studies in sample size—$n = 8$ in their study versus $n = 47$ in the present study—or in imaging method, confocal microscopy in

the present study versus light microscopy in the previous study.

When the relationship between bursting neurons and either cell morphology or discharge pattern was examined, some interesting correlations were found. The most striking observation was that fusiform and pyramidal neurons never exhibited rhythmic bursting (0 of 12 neurons for both). Although only 3 of 47 labeled neurons showed rhythmic bursting, they were all seen in multipolar neurons. The tendency of a neuron only to show rhythmic bursting based on firing pattern indicated that most rhythmic bursting neurons were associated with tonic or DF neurons (13 and 7 of 21 neurons, respectively), in contrast to phasic and SS neurons, which seldom exhibited rhythmic burst discharge (1 and none of 21 neurons, respectively). This likely resulted from the strong outward rectification observed in these neurons.

Intrinsic bursting SupV neurons, regardless of whether they are actually critical for oral-motor rhythm formation or are part of a network controlling oral-motor pattern generation, could be more important in reinforcing or facilitating the timing of information transferred within the network (Kiehn et al., 1996; Feldman and Del Negro, 2006). As such, multipolar bursting neurons with tonic or DF properties would impart robustness to the network output, thus increasing the dynamic range in output frequency and imparting greater stability to the network rhythms generated (Purvis et al., 2007). Development of model preparations that provide the ability to record the output of the oral-motor network during rhythmic activity and to do detailed electrophysiological analysis of putative CPG neurons, similar to that available for locomotor and respiratory systems (Ramirez et al., 1997; Latham et al., 2000b; Darbon et al., 2002, 2004; Del Negro et al., 2002) is a necessary starting point for characterizing oral-motor pattern generators.

REFERENCES

Boehmer G, Greffrath W, Martin E, Hermann S. 2000. Subthreshold oscillation of the membrane potential in magnocellular neurones of the rat supraoptic nucleus. J Physiol 526(Pt 1):115–128.

Bourque MJ, Kolta A. 2001. Properties and interconnections of trigeminal interneurons of the lateral pontine reticular formation in the rat. J Neurophysiol 86:2583–2596.

Bracci E, Centonze D, Bernardi G, Calabresi P. 2003. Voltage-dependent membrane potential oscillations of rat striatal fast-spiking interneurons. J Physiol 549(Pt 1):121–130.

Brocard F, Verdier D, Arsenault I, Lund JP, Kolta A. 2006. Emergence of intrinsic bursting in trigeminal sensory neurons parallels the acquisition of mastication in weanling rats. J Neurophysiol 96:2410–2424.

Chandler SH, Hsaio CF, Inoue T, Goldberg LJ. 1994. Electrophysiological properties of guinea pig trigeminal motoneurons recorded in vitro. J Neurophysiol 71(1):129–145.

Chandler SH, Tal M. 1986. The effects of brain stem transections on the neuronal networks responsible for rhythmical jaw muscle activity in the guinea pig. J Neurosci 6:1831–1842.

Coetzee WA, Amarillo Y, Chiu J, Chow A, Lau D, McCormack T, Moreno H, Nadal MS, Ozaita A, Pountney D, Saganich M, Vega-Saenz de Miera E, Rudy B. 1999. Molecular diversity of K+ channels. Ann N Y Acad Sci 868:233–285.

Darbon P, Scicluna L, Tscherter A, Streit J. 2002. Mechanisms controlling bursting activity induced by disinhibition in spinal cord networks. Eur J Neurosci 15(4):671–683.

Del Negro CA, Chandler SH. 1997. Physiological and theoretical analysis of K+ currents controlling discharge in neonatal rat mesencephalic trigeminal neurons. J Neurophysiol 77:537–553.

Del Negro CA, Hsiao CF, Chandler SH. 1999. Outward currents influencing bursting dynamics in guinea pig trigeminal motoneurons. J Neurophysiol 81:1478–1485.

Del Negro CA, Koshiya N, Butera RJ Jr, Smith JC. 2002. Persistent sodium current, membrane properties and bursting behavior of pre-botzinger complex inspiratory neurons in vitro. J Neurophysiol 88:2242–2250.

Donga R, Lund JP. 1991. Discharge patterns of trigeminal commissural last-order interneurons during fictive mastication in the rabbit. J Neurophysiol 66:1564–1578.

Feldman JL, Del Negro CA. 2006. Looking for inspiration: new perspectives on respiratory rhythm. Nat Rev Neurosci 7:232–242.

Goldberg LJ, Chandler SH. 1990. Central mechanisms of rhythmic trigeminal activity. In: Taylor A, editor. Neurophysiology of jaws and teeth. London: Macmillan. p 268–321.

Goldberg LJ, Nakamura Y. 1968. Lingually induced inhibition of masseteric motoneurones. Experientia 24:371–373.

Hamam BN, Amaral DG, Alonso AA. 2002. Morphological and electrophysiological characteristics of layer V neurons of the rat lateral entorhinal cortex. J Comp Neurol 451(1):45–61.

Hsiao CF, Chandler SH. 1995. Characteristics of a fast transient outward current in guinea pig trigeminal motoneurons. Brain Res 695:217–226.

Hsiao CF, Chandler SH. 2003. Discharge characteristics and membrane properties of interneurons in the rat supratrigeminal nucleus. Soc Neurosci Abstr 29:491, 499.

Hsiao CF, Del Negro CA, Trueblood PR, Chandler SH. 1998. Ionic basis for serotonin-induced bistable membrane properties in guinea pig trigeminal motoneurons. J Neurophysiol 79:2847–2856.

Inoue T, Chandler SH, Goldberg LJ. 1994. Neuropharmacological mechanisms underlying rhythmical discharge in trigeminal interneurons during fictive mastication. J Neurophysiol 71:2061–2073.

Inoue T, Masuda Y, Nagashima T, Yoshikawa K, Morimoto T. 1992. Properties of rhythmically active reticular neurons around the trigeminal motor nucleus during fictive mastication in the rat. Neurosci Res 14:275–294.

Izhikevich EM, Desai NS, Walcott EC, Hoppensteadt FC. 2003. Bursts as a unit of neural information: selective communication via resonance. Trends Neurosci 26:161–167.

Kamogawa H, Manabe K, Kondo M, Naito K. 1994. Supra- and juxtatrigeminal inhibitory premotor neurons with bifurcating axons projecting to masseter motoneurons on both sides. Brain Res 639(1): 85–92.

Khakh BS, Henderson G. 1998. Hyperpolarization-activated cationic currents (Ih) in neurones of the trigeminal mesencephalic nucleus of the rat. J Physiol 510(Pt 3):695–704.

Kidokoro Y, Kubota K, Shuto S, Sumino R. 1968. Possible interneurons responsible for reflex inhibition of motoneurons of jaw-closing muscles from the inferior dental nerve. J Neurophysiol 31:709–716.

Kiehn O, Johnson BR, Raastad M. 1996. Plateau properties in mammalian spinal interneurons during transmitter-induced locomotor activity. Neuroscience 75(1):263–273.

Kogo M, Funk GD, Chandler SH. 1996. Rhythmical oral-motor activity recorded in an in vitro brainstem preparation. Somatosens Mot Res 13(1): 39–48.

Latham PE, Richmond BJ, Nirenberg S, Nelson PG. 2000. Intrinsic dynamics in neuronal networks. II. experiment. J Neurophysiol 83:828–835.

Li JL, Wu SX, Tomioka R, Okamoto K, Nakamura K, Kaneko T, Mizuno N. 2005. Efferent and afferent connections of GABAergic neurons in the supratrigeminal and the intertrigeminal regions. An immunohistochemical tract-tracing study in the GAD67-GFP knock-in mouse. Neurosci Res 51(1):81–91.

Lisman JE. 1997. Bursts as a unit of neural information: making unreliable synapses reliable. Trends Neurosci 20(1):38–43.

Lund JP. 1991. Mastication and its control by the brain stem. Crit Rev Oral Biol Med 2(1):33–64.

McCormick DA, Pape HC. 1990. Properties of a hyperpolarization-activated cation current and its role in rhythmic oscillation in thalamic relay neurones. J Physiol 431:291–318.

Migliore M, Shepherd GM. 2002. Emerging rules for the distributions of active dendritic conductances. Nat Rev Neurosci 3:362–370.

Min MY, Hsu PC, Yang HW. 2003. The physiological and morphological characteristics of interneurons caudal to the trigeminal motor nucleus in rats. Eur J Neurosci 18:2981–2998.

Minkels RF, Juch PJ, van Willigen JD. 1995. Interneurones of the supratrigeminal area mediating reflex inhibition of trigeminal and facial motorneurones in the rat. Arch Oral Biol 40:275–284.

Miyazaki R, Luschei ES. 1987. Responses of neurons in nucleus supratrigeminalis to sinusoidal jaw movements in the cat. Exp Neurol 96(1): 145–157.

Mizuno N. 1970. Projection fibers from the main sensory trigeminal nucleus and the supratrigeminal region. J Comp Neurol 139:457–471.

Mizuno N, Yasui Y, Nomura S, et al 1983. A light and electron microscopic study of premotor neurons for the trigeminal motor nucleus. J Comp Neurol 215:290–298.

Nakamura Y, Katakura N. 1995. Generation of masticatory rhythm in the brainstem. Neurosci Res 23(1):1–19.

Paz JT, Deniau JM, Charpier S. 2005. Rhythmic bursting in the cortico-subthalamo-pallidal network during spontaneous genetically determined spike and wave discharges. J Neurosci 25:2092–2101.

Prescott SA, De Koninck Y. 2002. Four cell types with distinctive membrane properties and morphologies in lamina I of the spinal dorsal horn of the adult rat. J Physiol 539(Pt 3):817–836.

Ramirez JM, Telgkamp P, Elsen FP, Quellmalz UJ, Richter DW. 1997. Respiratory rhythm generation in mammals: synaptic and membrane properties. Respir Physiol 110(2–3):71–85.

Reboreda A, Sanchez E, Romero M, Lamas JA. 2003. Intrinsic spontaneous activity and subthreshold oscillations in neurones of the rat dorsal column nuclei in culture. J Physiol 551(Pt 1):191–205.

Reyes A. 2001. Influence of dendritic conductances on the input-output properties of neurons. Annu Rev Neurosci 24:653–675.

Rokx JT, van Willigen JD, Juch PJ. 1986. Bilateral brainstem connections of the rat supratrigeminal region. Acta Anat (Basel) 127(1):16–21.

Roper P, Callaway J, Armstrong W. 2004. Burst initiation and termination in phasic vasopressin cells of the rat supraoptic nucleus: a combined mathematical, electrical, and calcium fluorescence study. J Neurosci 24:4818–4831.

Sandler VM, Puil E, Schwarz DW. 1998. Intrinsic response properties of bursting neurons in the nucleus principalis trigemini of the gerbil. Neuroscience 83:891–904.

Smith M, Perrier JF. 2006. Intrinsic properties shape the firing pattern of ventral horn interneurons from the spinal cord of the adult turtle. J Neurophysiol 96:2670–2677.

Szucs P, Odeh F, Szokol K, Antal M. 2003. Neurons with distinctive firing patterns, morphology and distribution in laminae V–VII of the neonatal rat lumbar spinal cord. Eur J Neurosci 17:537–544.

Tanaka S, Kogo M, Chandler SH, Matsuya T. 1999. Localization of oral-motor rhythmogenic circuits in the isolated rat brainstem preparation. Brain Res 821(1):190–199.

Tanaka S, Wu N, Hsaio CF, Turman J Jr, Chandler SH. 2003. Development of inward rectification and control of membrane excitability in mesencephalic v neurons. J Neurophysiol 89:1288–1298.

Turman J Jr, Chandler SH. 1994a. Immunohistochemical evidence for GABA and glycine-containing trigeminal premotoneurons in the guinea pig. Synapse 18(1):7–20.

Turman JE Jr, Ajdari J, Chandler SH. 1999. NMDA receptor NR1 and NR2A/B subunit expression in trigeminal neurons during early postnatal development. J Comp Neurol 409:237–249.

Turman JE Jr, Chandler SH. 1994b. Immunohistochemical localization of glutamate and glutaminase in guinea pig trigeminal premotoneurons. Brain Res 634(1):49–61.

Urbani A, Belluzzi O. 2000. Riluzole inhibits the persistent sodium current in mammalian CNS neurons. Eur J Neurosci 12:3567–3574.

Westberg K, Clavelou P, Sandstrom G, Lund JP. 1998. Evidence that trigeminal brainstem interneurons form subpopulations to produce different forms of mastication in the rabbit. J Neurosci 18:6466–6479.

Westneat MW, Hall WG. 1992. Ontogeny of feeding motor patterns in infant rats: an electromyographic analysis of suckling and chewing. Behav Neurosci 106:539–554.

Wu N, Enomoto A, Tanaka S, Hsiao CF, Nykamp DQ, Izhikevich E, Chandler SH. 2005. Persistent sodium currents in mesencephalic v neurons participate in burst generation and control of membrane excitability. J Neurophysiol 93:2710–2722.

Wu N, Hsiao CF, Chandler SH. 2001. Membrane resonance and subthreshold membrane oscillations in mesencephalic V neurons: participants in burst generation. J Neurosci 21:3729–3739.

Yasui Y, Itoh K, Mitani A, Takada M, Mizuno N. 1985. Cerebral cortical projections to the reticular regions around the trigeminal motor nucleus in the cat. J Comp Neurol 241:348–356.